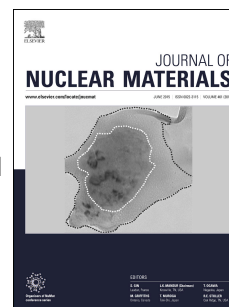


Accepted Manuscript

Nanoindentation study of the combined effects of crystallography, heat treatment and exposure to high-flux deuterium plasma in tungsten

Y. Zayachuk, D.E.J. Armstrong, K. Bystrov, S. Van Boxel, T. Morgan, S.G. Roberts



PII: S0022-3115(16)31122-9

DOI: [10.1016/j.jnucmat.2017.01.026](https://doi.org/10.1016/j.jnucmat.2017.01.026)

Reference: NUMA 50087

To appear in: *Journal of Nuclear Materials*

Received Date: 15 November 2016

Revised Date: 21 December 2016

Accepted Date: 15 January 2017

Please cite this article as: Y. Zayachuk, D.E.J. Armstrong, K. Bystrov, S. Van Boxel, T. Morgan, S.G. Roberts, Nanoindentation study of the combined effects of crystallography, heat treatment and exposure to high-flux deuterium plasma in tungsten, *Journal of Nuclear Materials* (2017), doi: 10.1016/j.jnucmat.2017.01.026.

This is a PDF file of an unedited manuscript that has been accepted for publication. As a service to our customers we are providing this early version of the manuscript. The manuscript will undergo copyediting, typesetting, and review of the resulting proof before it is published in its final form. Please note that during the production process errors may be discovered which could affect the content, and all legal disclaimers that apply to the journal pertain.

Nanoindentation study of the combined effects of crystallography, heat treatment and exposure to high-flux deuterium plasma in tungsten

Y. Zayachuk^{a, b} ×, D. E. J. Armstrong^a, K. Bystrov^c, S. Van Boxel^b, T. Morgan^c and S. G. Roberts^{a, b}

^aDepartment of Materials, University of Oxford, Parks Road, Oxford OX1 3PH, UK

^bCulham Centre for Fusion Energy, Culham Science Centre, Abingdon OX14 3DB, UK

^cFOM Institute DIFFER- Dutch Institute for Fundamental Energy Research, Trilateral Euregio Cluster, De Zaale 20, 3612 AJ Eindhoven, the Netherlands

×Corresponding author's e-mail: yevhen.zayachuk@materials.ox.ac.uk

Abstract: tungsten samples were heat-treated to achieve partial recrystallization and exposed to high ion flux deuterium plasma at different temperatures and fluences. Continuous stiffness nanoindentation measurements of near-surface hardness were performed in the grains of specific annealing states and of specific crystallographic orientation, determined by electron backscatter diffraction (EBSD); indentation pile-up was investigated using surface profilometry. Bulk hardness of unexposed tungsten does not strongly depend on grain orientation, but depends on the annealing state of the grain, with values between ~4.3 GPa for recrystallized grains and ~5.5 for non-recrystallized ones. Grains with <111> surface normal orientation feature the least pile-up, while grains with <001> orientation the most; pile-up also depends on the annealing state, being generally lower in recrystallized grains. Plasma exposure leads to the increase of hardness, most significantly near the surface. The width of plasma-affected zone increases with the increase of exposure temperature and fluence, as well in recrystallized grains, correlating with the increase of diffusion depth. Plasma exposure does not lead to the emergence of orientation-dependence of hardness. Both indentation pile-up and near-surface indentation pop-ins are generally suppressed by plasma exposure.

Keywords: nanoindentation; EBSD; tungsten; annealing; deuterium plasma.

1. Introduction

Tungsten is one of the main candidate plasma-facing materials to be used in future fusion reactors. Exposure of tungsten to a high ion flux plasma of hydrogen isotopes under conditions comparable to those at the plasma-wall boundary in a fusion reactor leads to a significant plasma-induced modification [1] [2], resulting in the enhancement of plasma-driven hydrogen isotope uptake [3]. Thus understanding the dynamics of plasma-induced material modification is important from the point of view of tritium retention in plasma-facing components, which is an important issue with regard to safety and operation of a fusion device [4].

Plasma-induced surface modification manifests itself in the formation of macroscopic sub-surface cavities, associated with surface blistering [5]. It is often reported that blistering process is non-uniform – micrographs of the plasma-exposed surfaces reveal regions of intense blistering directly neighbouring blister-free regions [6]. Orientation imaging using electron backscatter diffraction (EBSD) revealed that these regions correspond to different grains and are separated by high-angle grain boundaries [7]. This non-uniformity might be correlated with differences in local grain-specific mechanical properties. Plasma-induced material modification may also change the local mechanical properties. The plasma effects are usually confined to the near-surface region extending at most to several microns in depth [8].

These considerations provided the motivation for the work presented here. Micromechanical testing methods allow grain specific measurements of mechanical properties [9], and at the same time enable measuring the depth dependence of mechanical properties in the relevant depth range [10]. Therefore we used a combination of Electron Backscatter Diffraction (EBSD), nanoindentation and surface profilometry in order to study the correlation between measured values of hardness and local crystallographic structure. EBSD was used to identify and characterize grains in the investigated polycrystalline material; nanoindentation was used to measure grain-specific hardness, profilometry was used to measure near-indent pile-up. Measurements were performed on pristine commercial material, and on material that had been exposed to fusion-relevant high-flux deuterium plasma, so that changes induced by such an exposure could be studied.

2. Experiment

The tungsten used in the study was procured from Goodfellow Metals (UK), as 99.95% pure material (main impurities being Mo, Pb, Si, all below 160 appm) in the form of a rod, 20 mm in diameter. Samples were produced by cutting 1mm thick slices from the rod with a diamond saw. Samples were mechanically ground with

SiC abrasive paper down to 2500 grit, then mechanically polished with 3 and 1 μm diamond suspension on NLH polishing cloths, and then electrochemically polished in 0.5 weight % NaOH water solution at 12 V. Finally, samples were heat-treated in vacuum ($\sim 10^{-5}$ mbar), being kept at 1700 K for 20 hours. Following heat treatment, the mean grain size, as determined by EBSD, was $\sim 200 \mu\text{m}$. Fig. 1 shows forward-scattered electron images of the post-annealing microstructure. Intragranular contrast differences in this image are indicative of the amount of internal substructure within the grains, so that featureless areas represent fully recrystallized grains; other grains still have internal strains after the heat treatment. This is similar to microstructures obtained at the same annealing temperature reported in [11], but in contrast to results from the annealing of ultra-high purity tungsten in [12] which showed full recrystallization and substantial grain growth after annealing at 1700K for 24 hours.

Fig. 1

Hardness measurements were performed in an Agilent MTS XP nanoindenter, using a diamond Berkovich tip calibrated on fused silica, using the continuous stiffness measurement (CSM) method. Depth-dependent values of hardness were extracted from load-displacement curves of individual indents using the Oliver-Pharr method [13].

Profilometry measurements were done using an Agilent G200 nanoindenter equipped with nanopositioning stage, which allows for the creation of quantitative 3D surface maps [14] by imaging the surface with the indenter tip.

In order to study the relationship between measured hardness data and local crystallographic structure, electron backscatter diffraction (EBSD) was performed with a Zeiss EVO electron microscope equipped with Bruker Quantax EBSD detector. Grains are identified in post processing as areas which are bounded by a continuous boundary with a misorientation of more than 15° .

Plasma exposures were performed in the linear plasma generator Pilot-PSI (FOM Institute DIFFER, Nieuwegein, the Netherlands) [15][16]. In this device the plasma is generated by a cascaded arc discharge. Electron temperature and density profiles (and therefore also particle and heat flux profiles) within the plasma beam are roughly Gaussian with a FWHM of ~ 1 cm. During the plasma exposure, the sample is fixed to a copper cooling plate by a clamping ring with internal diameter of 16 mm; the surface temperature of the sample is controlled by the balance between incoming heat flux and rate of heat removal by water cooling. Good thermal contact between a sample a cooling plate and is provided by a soft grafoil interlayer. Sample temperature returns to room temperature in ~ 2 s after plasma is stopped. The ion flux arriving at the surface of the specimen is calculated from the electron temperature and density measured by Thomson scattering, and the surface temperature of each specimen is monitored by an IR camera FLIR SC7500MB, with the typical accuracy of $\pm 15^\circ$.

Pilot-PSI operates in a pulsed regime, which means that in order to accumulate high ion fluences it is necessary to perform several sequential exposures. Each of these exposures (referred to in the following as “reference shots”) was performed under identical conditions, with the maximum D ion flux of $5\text{--}8 \times 10^{23} \text{ m}^{-2}\text{s}^{-1}$, a time duration of 70 s/shot, ion fluence (calculated in the location of maximum ion flux) of $\sim 5 \times 10^{25} \text{ m}^{-2}$ /shot, maximum surface temperature of ~ 450 K in the low-temperature regime and ~ 650 K in the high-temperature regime, and ion energy (determined by the sample bias voltage) of 50 eV.

3. Results and discussion

3.1 Nanoindentation on heat-treated tungsten

In order to characterize the changes in the state of the material’s surface as a result of plasma exposure, measurements on “reference” samples, were performed first. These samples were not exposed to the plasma but underwent the same thermal history as the exposed ones.

Fig. 2a shows the hardness of the reference material, measured for multiple indents, in the locations with local normal orientations close (within $\sim 10^\circ$) to $\langle 111 \rangle$, $\langle 101 \rangle$ and $\langle 001 \rangle$ axes. The values of hardness shown are averaged over the indenter depth range 1000 – 1800 nm. This depth range was chosen to be outside of the range of significant size effects [17], so as to characterize true bulk value of hardness. There is no dependence on hardness as a function of grain orientation. This is consistent with the reported results of similar measurements [18][19]. However the hardness data are split into two distinct groups, one centered around 5.5 GPa (denoted by filled black symbols) and another centered around ~ 4.3 GPa (hollow red symbols).

Fig. 2

Fig. 3a presents an example of an EBSD orientation map at the position of a typical indent array, including indents with values of hardness characteristic of both the high-hardness (denoted by circles) and low-hardness

sets. The high-angle grain boundary does not correspond to the boundary between the regions with different values of hardness, indicating that this difference is not related to grain orientation.

Using EBSD it is possible to represent orientation data as a misorientation map. In this mode, an average orientation of each grain is determined, and each individual pixel is assigned a value, represented by a color code, of the misorientation angle between the local orientation and the average orientation of the grain. Fig. 3b presents the misorientation map for the same area as shown in Fig 3a; it is evident that the regions with low and high values of hardness correspond to the regions with low and high values of internal misorientation.

Fig. 3

In order to quantify this behavior, we define a parameter we call “misorientation factor” as the value of the misorientation angle averaged over all the indexed locations within a given area. For the indentations, the misorientation factor is calculated as the average value of the misorientation angle of all indexed locations in a rectangular area of $15\ \mu\text{m}$ by $15\ \mu\text{m}$ with the indent in the centre, for example as indicated by the rectangle in Fig. 3b. Fig. 2b shows hardness as a function of the local misorientation factor. There is a clear trend. Indents located in grains, or parts of grains, with low internal misorientation give values of hardness around $\sim 4.4\ \text{GPa}$, while those in areas with a high misorientation factor have hardness close to $\sim 5.5\ \text{GPa}$. The transition from low-hardness behavior to high-hardness behavior occurs at a misorientation factor value of $\sim 1^\circ$, over a very narrow range of values. Within the region of high misorientation and high hardness, even though the values of misorientation factor varies widely, there is no correlation between hardness and misorientation factor. As noted above, the degree of internal misorientation indicates the annealing state of the grain. Recrystallized grains correspond to low misorientation factor and deformed ones to high, and thus recrystallized grains have low hardness and deformed grains have high hardness.

Pile-up around the indents was studied using the profilometry technique. Small, $400\ \text{nm}$ deep, indents were used for this study. The influence of grain orientation and deformation state of the grain on pile-up dynamics was investigated, comparing the pile-up around indents in deformed and recrystallized grains with surface normal orientations close to $\langle 111 \rangle$, $\langle 101 \rangle$ and $\langle 001 \rangle$.

Fig. 4a presents the typical profiles of indents in deformed grains in the reference sample. There is a strong orientation dependence of the height of the pile-up. Grains with surface normal close to $\langle 111 \rangle$ feature the smallest amount of pile-up – $400\ \text{nm}$ deep indents create pile-up of $\sim 40\ \text{nm}$ height, while those in grains with $\langle 001 \rangle$ orientation yield the strongest pile-up – up to $\sim 80\ \text{nm}$ in height from indents of the same depth. Indents in grains with $\langle 101 \rangle$ orientation fall in between with $\sim 60\ \text{nm}$ of pile-up height. This is consistent with the data presented in [20], where similar correlation between surface normal orientation and height of pile-up was observed in spherical microindentation measurements on single crystal tungsten.

Fig. 4

Fig. 4b presents similar profiles for indents in recrystallized grains in the reference sample. Crystallographic dependence of pile-up is still present, and indents in grains with $\langle 001 \rangle$ surface normal have the strongest pile up. However, pile-up heights are lower than around indents in deformed grains. For an indent depth of $400\ \text{nm}$, pile-up height in grains with $\langle 111 \rangle$ and $\langle 101 \rangle$ surface normals is $\sim 20\ \text{nm}$, while in $\langle 001 \rangle$ grain it is $\sim 40\ \text{nm}$.

3.2 Nanoindentation on plasma-exposed tungsten

Similar nanoindentation measurements were performed on plasma-exposed samples. In order to characterize the material modification induced by the plasma exposure, depth dependences of hardness measured on the exposed samples were analyzed. Since it was established that in the reference material deformed and recrystallized grains feature significantly different values of hardness, data from the two different grain types were considered separately.

Fig. 5 presents depth dependence of hardness for reference and exposed samples, measured on deformed grains. These depth dependences were calculated each by averaging curves yielded by 16 indentations. Comparison of data taken from different indentations placed on different grains show significant scatter, thus error bars are rather large. Nevertheless, it is evident that plasma exposure leads to a noticeable increase of hardness.

Fig. 5

Comparison of the curves for samples exposed at the same temperature but different fluences indicates that: (1) Hardness of the near-surface layer does not appear to be affected by fluence: despite a $20\times$ difference in ion fluence ($1\ \text{shot}: 5 \times 10^{25}$ versus $20\ \text{shots}: 10^{27}\ \text{m}^{-2}$), similar values of hardness were found within the first $\sim 250\ \text{nm}$

from the surface. (2) Increase of exposure fluence leads to the expansion of the affected zone. As indentation depth increases, the hardness difference between the sample exposed to 1 shot and the reference sample becomes smaller, and at the depth of ~2000 nm their values of hardness become identical. However, the sample exposed to 20 shots features increased hardness to larger depth; for the sample exposed at 450 K all the way down to the end of the probed range of 2000 nm.

There is a notable difference between low- and high-temperature exposures: in high-temperature exposures the increased values of hardness approach those of the reference sample at shallower depths than in low-temperature exposures. The difference is especially noticeable for long exposures (20 shots): by ~1800 nm depth, the hardness of the sample exposed at 450 K has reached the reference value, while the hardness of the sample exposed to the same fluence at 650 K is above the reference value over the whole probed depth range of 2000 nm. However, the maximum values of increased hardness, in the very near-surface region, are essentially identical for both exposure temperatures, as well as for both exposure fluences.

Similar measurements were performed on recrystallized grains. Fig. 6 presents the comparison of the corresponding depth dependences of hardness for different fluences and temperatures. Hardness increases after plasma exposure; and the difference between the reference and exposed samples is more pronounced than in the deformed grains. However, here the plasma-affected zone seems to extend to much larger depths. In both 1 and 20 shots exposures, both in low-temperature and high-temperature exposures, the plasma-affected zone extends beyond the measurement range of 2000 nm, with the factor of 20 increase of fluence leading to only marginal increase in hardness throughout the whole measurement range in 450 K exposure; increase of hardness with fluence in 650 K exposure is more pronounced. Again this implies that the plasma-affected zone is much wider than the maximum probed range, so that the region where the difference between different fluences appears is too deep to be observed.

Fig. 6

It is known that irradiation of tungsten by ions, including protons, leads to hardening [21][12][22]. However, in such experiments, the ion energy is typically in the range from tens of keV to tens of MeV, while the ion flux is rather low, of the order of $\sim 10^{19} \text{ m}^{-2}\text{s}^{-1}$. Such high energies produce displacement damage in the form of vacancy clusters and dislocation loops, whose interaction with moving dislocations leads to hardening [23]. In the experiments reported here, the ion energy was ~50 eV, much lower than that required to create displacement damage in tungsten by deuterium ions (~940 eV [24]). On the other hand, the ion flux is much higher – $\sim 10^{24} \text{ m}^{-2}\text{s}^{-1}$ – than in typical high-energy experiments. Present findings are consistent with those reported in [25], where implemented experimental conditions were similar.

Deuterium is extremely mobile in tungsten, even at room temperature (the generally accepted value of Frauenfelder diffusivity is $4.1 \times 10^{-7} \exp(-0.39/kT) \text{ m}^2\text{s}^{-1}$ [26]). Thus during the exposure its depth distribution is not determined by the implantation depth of the primary ions, but rather by thermal diffusion following implantation, thermalization and neutralization of deuterium ions. The diffusion depth profile is governed by Fick's second law with the boundary condition of constant surface concentration [27], that is

$$C(x, t) = C_0 \operatorname{erfc}\left(\frac{x}{\lambda}\right) \quad (\text{Eq. 1})$$

where C is concentration, x depth, t time, C_0 constant surface concentration, with characteristic diffusion depth λ determined as

$$\lambda(t) = \sqrt{Dt} \quad (\text{Eq. 2})$$

where D is diffusivity, which in turn is determined as

$$D = D_0 \exp\left(-\frac{E_{\text{act}}}{kT}\right) \quad (\text{Eq. 3})$$

where D_0 is pre-exponential factor, E_{act} is activation energy for diffusion, and T temperature.

Thus, diffusion depth scales both with temperature and with time duration. This can be correlated with the changes of depth dependences of hardness with changing exposure duration (Fig. 5 and Fig. 6). The increase of exposure duration (or fluence) leads to the increase of the width of plasma-affected zone. This can be interpreted as hardness increase in the region where deuterium is present, and thus when deuterium reaches deeper due to thermal diffusion, the region of increased hardness is wider as well. Notably this hardened region is not associated with the implantation depth: according to SRIM calculations [28], implantation depth at 50 eV is in the order of ~2 nm, which is incomparable with the width of plasma-affected region. It can be seen as if the diffusing deuterium hardens the tungsten matrix as it moves into the material. This can also be compared to measurements of depth distribution of plasma-induced modification measured by monitoring the enhancement of

deuterium retention by plasma exposure [29]. Exposure of tungsten by deuterium plasma at conditions similar to those used in this study results in a zone of enhanced retention at least 8 μm deep.

Hardening must be associated with generation of crystallographic defects [30]. Since deuterium creating a zone of enhanced hardness is thermalized, this cannot be attributed to displacement damage. Instead, a mechanism involving the formation of defects, such as dislocations or dislocation loops, due to the supersaturation of solute deuterium (such as proposed in [31]), can be suggested.

The drop of increased values of hardness with depth occurs more slowly in the recrystallized grains, which indicates that the plasma-affected zone is wider in them. This indicates that diffusion transport of deuterium is different in recrystallized and deformed grains. It is known that crystallographic defects with binding energies for hydrogen isotopes that is higher than diffusion activation energy can operate as trapping sites [32]. The presence of such trapping sites hinders diffusion reducing effective diffusivity [33][34]:

$$D_{eff} = \frac{D}{1+\alpha} \quad (Eq. 4)$$

$$\alpha = c_t \exp\left(\frac{E_b}{kT}\right) \quad (Eq. 5)$$

where D_{eff} is effective diffusivity, c_t concentration of traps and E_b binding energy of traps.

It has been shown that in tungsten dislocations can act as trapping sites for diffusing deuterium [35]. Since recrystallized grains have less internal structure, in particular lower density of dislocations, and since according to equations 4 and 5 effective diffusivity is higher when concentration of traps is lower, it is reasonable to assume that in such grains deuterium trapping is less efficient and therefore effective diffusivity higher; as a result, diffusion depth for a given exposure time and temperature is higher as well.

These findings can be compared to those presented in [19], where results of nanoindentation measurements were performed on single crystal tungsten exposed to deuterium plasma and no influence of plasma exposure on hardness was observed. This indicates that exposure conditions used in the present study result in the generation of noticeable plasma-induced modification, while those used in [19] do not. An essential difference between the conditions of two experiments was ion flux density: $\sim 10^{24} \text{ m}^{-2}\text{s}^{-1}$ in this study and $\sim 10^{20} \text{ m}^{-2}\text{s}^{-1}$ in [19]. Thus, observed discrepancy in hardness might be explained by the “flux effect” reported in [36], which manifests itself in the generation of plasma-induced defects being active at high-flux exposure conditions and almost non-existent at low-flux conditions.

Detailed measurements of hardness in the near-surface region of the reference samples feature a high spike in the depth range of $\sim 50 \text{ nm}$, for both recrystallized and deformed grains. Comparison with corresponding load-displacement curves indicates that it is associated with the occurrence of pop-in. This reveals a fundamental difference between reference and plasma-exposed samples, in addition to general hardening. Fig. 7 compares the unexposed and exposed samples, showing that while the unexposed samples feature a high spike in the range down to $\sim 50 \text{ nm}$, exposed ones do not, and thus plasma exposure suppresses a near-surface pop-in. This is similar to the effect of low-flux plasma exposure reported in [19] and high energy tungsten ion and helium ion irradiation [12]. Such pop-ins are attributed to defect generation during the indentation process, in particular to homogeneous nucleation of dislocation loops under the indenter tip. Thus, it can be concluded that plasma exposure suppresses this nucleation. This can be explained by the additional difficulty of generation of additional dislocation structures in the presence of higher dislocation density resulting from plasma-induced hardening. Prior to such pop-ins the material response is fully elastic, suggesting that the onset of permanent plastic deformation is easier in the plasma exposed material while the material itself being harder.

Fig. 7

Orientation dependence of hardness was studied for plasma-exposed samples as well, in order to determine whether any orientation effect emerges as a result of plasma exposure. It should be noted that plasma exposure strongly degrades the quality of the recorded diffraction patterns. This is demonstrated by the example of Fig. 8, which presents the comparison between the patterns in the parts of the exposed and unexposed (due to being covered by the clamping ring) regions of the same grain. It is evident, however, that even after the plasma exposure pattern quality is still sufficient to perform indexing and determine orientation (and internal misorientation) of the grains.

Fig. 8

Since the effects of plasma exposure are the strongest near the surface (see Fig. 5 and 6), near-surface values of hardness were used. Fig. 9 compares the values of hardness averaged over the 300 – 400 nm depth range for the reference and plasma-exposed sample (20 reference plasma shots – $\sim 10^{27} \text{ m}^{-2}$ accumulated fluence, 450 K), plotted as a function of grain normal orientation and of misorientation factor. Hollow symbols denote the

low-misorientation locations, filled symbols correspond to high-misorientation locations. In reference samples, in this depth range there appears a certain dependence of hardness on orientation, especially noticeable in low-hardness recrystallized grains. For such grains, hardness of the areas with surface normal close to $\langle 111 \rangle$ appear to be the lowest, ~ 4.9 GPa, whereas areas close to $\langle 001 \rangle$ have the highest hardness of ~ 5.5 GPa. Unlike the reference sample, in the exposed one there is still no orientation dependence of hardness.

Fig. 9

In order to determine the impact of plasma exposure on local plasticity, profilometry measurements of pile-up were performed on the indents placed in deformed and recrystallized grains with surface normal close to $\langle 111 \rangle$, $\langle 101 \rangle$ and $\langle 001 \rangle$, of the exposed samples. Fig. 10a presents the results of profilometry of 400 nm deep indents made in deformed grains in the sample exposed to 1 shot at 450 K. The orientation dependence of pile-up is still noticeable, with $\langle 001 \rangle$ orientation featuring the highest pile-up, and $\langle 111 \rangle$ the lowest, but in general pile-up in the exposed sample is significantly suppressed compared to the reference. In particular, grains with $\langle 111 \rangle$ surface normal feature essentially no pile-up at all, compared to ~ 40 nm pile-up around the indent of similar depth in analogous grain of reference sample. Other orientations feature smaller heights of pile-up as well, values for $\langle 101 \rangle$ grain being reduced from ~ 60 to ~ 30 nm, and for $\langle 001 \rangle$ from ~ 80 to ~ 40 nm. Fig. 10b presents a similar comparison for recrystallized grains. They feature lower pile-up as compared to deformed ones, as was the case also with reference samples. In grains with both $\langle 111 \rangle$ and $\langle 101 \rangle$ surface normal pile-up is completely suppressed; in grains with $\langle 001 \rangle$ height of pile-up is ~ 40 nm for 400 nm deep indent, close to the original value for the reference sample.

Fig. 10

As shown by Oliver and Pharr [37] the degree of pile up around indentations in metals depends on the ratio of modulus to hardness (E/H) and the capacity of the material to work harden. Generally, a larger value of E/H suggests more significant pile up, and the more capacity a material has to work-harden the lower the degree of pile up. The changes seen in this tungsten between recrystallized and deformed grains and between materials that has been exposed to plasma or not show exactly this. The unexposed tungsten showed more pile up in the deformed grains which had a lower E/H ratio than the recrystallized grains which have a higher E/H ratio. This is due to the lower work hardening capability of the deformed grains which results in a more constrained plastic zone and thus more pile up even though it has the lower E/H ratio. As can be seen in Fig. 6 the hardness of the tungsten increases by 1 GPa after exposure to 20 plasma shots. This represents a change E/H ratio from 66 to 57 (assuming 400 GPa modulus of tungsten), with a corresponding decrease in the observed pile up.

4. Summary

The main experimental observations reported in this paper can be divided into ones related to the properties of the reference material and the effects of heat treatment, and ones related to the effects of plasma exposure, and summarized as follows:

Properties of the reference material:

- (1) There is a grain dependence of bulk hardness in partially recrystallized tungsten. However, it is not directly related to the grain orientation. Rather, it depends on whether a grain is recrystallized or not, reflected in the corresponding value of the misorientation factor. Values of misorientation factor below $\sim 1^\circ$ lead to hardness values of ~ 4.3 GPa while those above $\sim 1^\circ$ - to hardness values of ~ 5.5 GPa.
- (2) There is a grain dependence of pile-up in tungsten. In partially recrystallized material, it is influenced by both general grain orientation and on annealing state of the grain. Grains with $\langle 111 \rangle$ surface normal orientation feature the least pile-up, while grains with $\langle 001 \rangle$ orientation the most. In general, pile-up is suppressed in recrystallized grains as compared to the deformed ones.

Effects of plasma exposure:

- (3) High-flux deuterium plasma exposure leads to hardening. The difference between the values of hardness for reference and exposed samples is highest close to the surface and decreases into the bulk. The width of plasma-affected zone increases with the increase of exposure temperature and fluence – that is, it can be correlated with the increase of diffusion depth. This suggests that hardening is associated with the propagation of diffusing deuterium during the plasma exposure.
- (4) Dynamics of plasma-induced hardening is different for deformed and recrystallized grains. In recrystallized grains the increased values of hardness drop to the reference values much slower, that is the plasma-affected

region is broader. This correlates with the fact that diffusivity is higher in recrystallized grains, so that during the exposure deuterium can propagate deeper into the material.

(5) Plasma exposure suppresses the indentation pile-up.

(6) Plasma exposure suppresses the indentation pop-in.

Acknowledgements

This work has been carried out within the framework of the EUROfusion Consortium and has received funding from the Euratom research and training programme 2014-2018 under grant agreement No 633053. The views and opinions expressed herein do not necessarily reflect those of the European Commission. D. Armstrong acknowledges support from the Royal Academy of Engineering in the form of a Research Fellowship

References

- [1] O. Ogorodnikova, J. Roth and M. Mayer, Deuterium retention in tungsten in dependence of the surface conditions, *J. Nucl. Mater.* 313–316 (2003) 469–77.
- [2] V. Alimov, J. Roth and M. Mayer, Depth distribution of deuterium in single- and polycrystalline tungsten up to depths of several micrometers, *J. Nucl. Mater.* 337–339 (2005) 619–23.
- [3] Y. Zayachuk, M.H.J. 't Hoen, P.A. Zeijlmans van Emmichoven, I. Uytdenhouten and G. van Oost, Deuterium retention in tungsten and tungsten–tantalum alloys exposed to high-flux deuterium plasmas, *Nucl. Fusion* 52 (2012) 103021.
- [4] R.A. Causey, Hydrogen isotope retention and recycling in fusion reactor plasma-facing components, *J. Nucl. Mater.* 300 (2002) 91–117.
- [5] M. Balden, S. Lindig, A. Manhard, J. You, D₂ gas-filled blisters on deuterium-bombarded tungsten, *J. Nucl. Mater.* 414 (2011) 69–72.
- [6] W. M. Shu, E. Wakai and T. Yamanishi, Blister bursting and deuterium bursting release from tungsten exposed to high fluences of high flux and low energy deuterium plasma. *Nucl. Fusion* 47 (2007), 201–209.
- [7] W. Shu, A. Kawasuso, Y. Miwa, E. Wakai, G. Luo, T. Yamanishi, Microstructure dependence of deuterium retention and blistering in the near-surface region of tungsten exposed to high flux deuterium plasmas of 38 eV at 315K, *Phys. Scr.* T128 (2007) 96–99.
- [8] S. Lindig, M. Balden, V. Kh. Alimov, T. Yamanishi, W. M. Shu and J. Roth, Subsurface morphology changes due to deuterium bombardment of tungsten, *Phys. Scr.* T138 (2009) 014040.
- [9] C. Fizanne-Michel, M. Cornen, P. Castany, I. Péron, T. Gloriant, Determination of hardness and elastic modulus inverse pole figures of a polycrystalline commercially pure titanium by coupling nanoindentation and EBSD techniques, *Mat. Sci. Eng. A*, 613 (2014) 159–162.
- [10] R. Kasada, Y. Takayama, K. Yabuuchi, A. Kimura, A new approach to evaluate irradiation hardening of ion-irradiated ferritic alloys by nano-indentation techniques, *Fus. Eng. Des.* 86 (2011) 2658–2661.
- [11] A. Manhard, K. Schmid, M. Balden, W. Jacob, Influence of the microstructure on the deuterium retention in tungsten, *J. Nucl. Mat.* 415 (2011) S632–S635.
- [12] D.E.J. Armstrong, X. Yi, E. A. Marquis, S. G. Roberts, Hardening of self ion implanted tungsten and tungsten 5-wt% rhenium, *J. Nucl. Mater.* 432 (2013) 428–436.
- [13] W.C. Oliver and G.M. Pharr, An improved technique for determining hardness and elastic modulus using load and displacement sensing indentation experiments, *J. Mater. Res.* 7, 1564 (1992).
- [14] P.A. Agee, Instrumented Indentation Testing with the Agilent Nano Indenter G200, Agilent Application note (2009).
- [15] G.J. van Rooij, V. P. Veremiyenko, W.J. Goedheer, B. de Groot, A.W. Kleyn, P.H.M. Smeets, T.W. Versloot, D.G. Whyte, R. Engeln, D.C. Schram, and N.J. Lopes Cardozo, Extreme hydrogen plasma densities achieved in a linear plasma generator, *Appl. Phys. Lett.* 90 (2007) 121501.
- [16] G. De Temmerman, J.J. Zielinski, S. van Diepen, L. Marot and M. Price, ELM simulation experiments on Pilot-PSI using simultaneous high flux plasma and transient heat/particle source, *Nucl. Fusion* 51 (2011) 73008.
- [17] W.D. Nix, H. Gao, Indentation size effects in crystalline materials: a law for strain gradient plasticity, *J. Mech. Phys. Solids*, 46 (1998), pp. 411–425.
- [18] J.J. Vlassak and W. D. Nix, Measuring the elastic properties of anisotropic materials by means of indentation experiments, *J. Mech. Phys. Solids*, 42 (1994) 1223–1245.
- [19] W.Z. Yao, P. Wang, A. Manhard, C.E. Krill III, J.H. You, Effect of hydrogen on the slip resistance of tungsten single crystals, *Materials Science & Engineering A* 559 (2013) 467–473.
- [20] W.Z. Yao, C.E. Krill III, B. Albinski, H.-C. Schneider, J.H. You, Plastic material parameters and plastic anisotropy of tungsten single crystal: a spherical micro-indentation study, *J Mater Sci* 49 (2014) 3705–3715.

- [21] S.A. Maloy, M.R. James, W. Sommer Jr., G.J. Willcutt Jr., M. Lopez, T.J. Romero, M.B. Toloczko, The effect of 800 MeV proton irradiation on the mechanical properties of tungsten at room temperature and at 475 C, *J. Nucl. Mater.* 343 (2005) 219–226.
- [22] T. Hwang, M. Fukuda, S. Nogami, A. Hasegawa, H. Usami, K. Yabuuchi, K. Ozawa, H. Tanigawa, Effect of self-ion irradiation on hardening and microstructure of tungsten, *Nucl. Mat. Eng.* 000 (2016) 1–6.
- [23] D.E.J. Armstrong, P.D. Edmondson, S.G. Roberts, Effects of sequential tungsten and helium ion implantation on nano-indentation hardness of tungsten, *Applied Physics Letters* 102 (2013), 251901.
- [24] A.D. Quastel, J.W. Davis, A.A. Haasz and R.G. Macaulay-Newcombe, Effect of post-D⁺-irradiation time delay and pre-TDS heating on D retention in single crystal tungsten, *J. Nucl. Mater.* 359 (2006) 8–16.
- [25] D. Terentyev, A. Bakaeva, T. Pardoen, A. Favache, E.E. Zhurkin, Surface hardening induced by high flux plasma in tungsten revealed by nano-indentation, *J. Nucl. Mater.* 476 (2016) 1–4.
- [26] J. Frauenfelder, Solution and diffusion of hydrogen in tungsten, *J. Vac. Sci. Technol.* 6 (1968) 388.
- [27] H. Mehrer, *Diffusion in solids*, Springer-Verlag Berlin Heidelberg 2007.
- [28] J.F. Ziegler, M.D. Ziegler, J.P. Biersack, SRIM – the stopping range of ions in matter, *Nucl. Instrum. Methods Phys. Res. B. Beam Interact. Mater. Atoms.* 268 (2010) 1818-1823.
- [29] Y. Zayachuk, A. Manhard, M.H.J. ‘t Hoen, W. Jacob, P.A. Zeijlmans van Emmichoven and G. van Oost, Depth profiling of the modification induced by high-flux deuterium plasma in tungsten and tungsten–tantalum alloys, *Nucl. Fusion* 54 (2014) 123013.
- [30] J. Gittus, *Irradiation effects in crystalline solids*, London: Applied Science Publishers LTD, 1978.
- [31] D. Terentyev, G. De Temmerman, T.W. Morgan, Y. Zayachuk, K. Lambrinou, B. Minov, A. Dubinko, K. Bystrov and G. Van Oost, Effect of plastic deformation on deuterium retention and release in tungsten, *J. App. Phys.* 117 (2015) 083302.
- [32] A. McNabb, P. K. Foster, A new analysis of the diffusion of hydrogen in iron and ferritic steels. *Trans. Met. Soc. AIME* 227 (1963) 618-27.
- [33] R. Oriani, The diffusion and trapping of hydrogen in steel, *Acta Met.*, 18 (1970).
- [34] H. J. Grabke, E. Riecke, Absorption and diffusion of hydrogen in steels, *Mater. Technol.* 34 (2000) 331 – 342.
- [35] O. V. Ogorodnikova, J. Roth, and M. Mayer, Ion-driven deuterium retention in tungsten, *J App. Phys.* 103 (2008) 034902.
- [36] Y. Zayachuk, A. Manhard, M.H.J. ‘t Hoen, W. Jacob, P.A. Zeijlmans van Emmichoven, G. Van Oost, The effect of ion flux on plasma-induced modification and deuterium retention in tungsten and tungsten–tantalum alloys, *J. Nucl. Mater.* 464 (2015) 69–72.
- [37] W.C. Oliver, G.M. Pharr, Measurement of hardness and elastic modulus by instrumented indentation: Advances in understanding and refinements to methodology, *J. Mater. Res.* 19 (2004) 1.

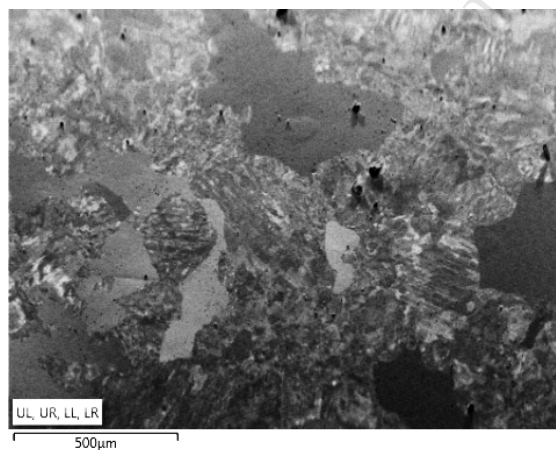


Fig. 1 Typical microstructures produced by heat treatment at 1700K for 20 hours.

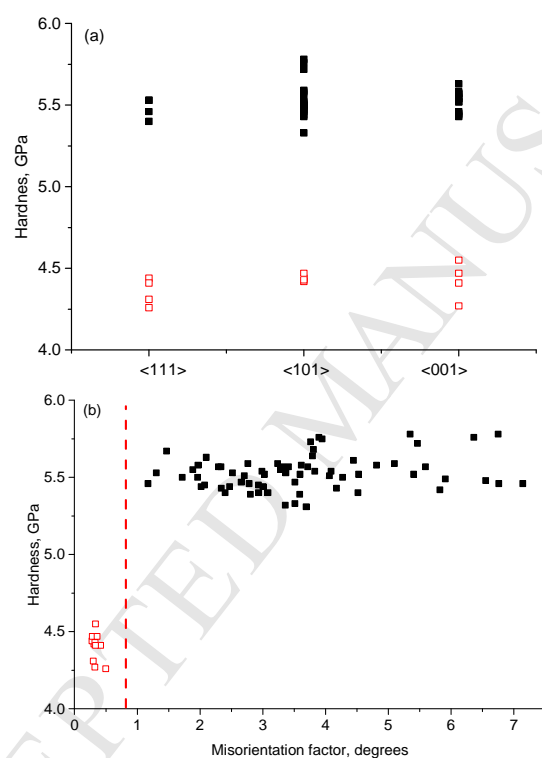


Fig. 2 Dependence of hardness for reference sample, averaged over the depth range of 1000 – 1800 nm, on (a) crystallographic orientation and (b) misorientation factor. Each data point corresponds to a single indent, black filled symbols correspond to high-hardness, red hollow ones to low-hardness indents.

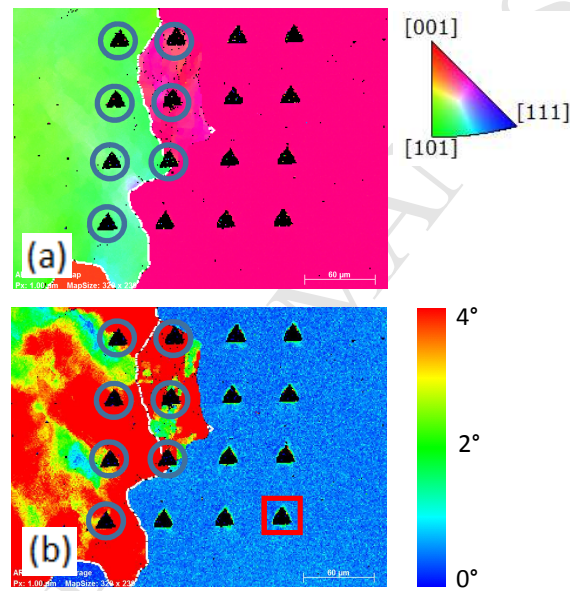


Fig. 3 EBSD (a) orientation and (b) misorientation map of the vicinity of a typical nanoindent array. White line denotes the grain boundaries as determined by 15° misorientation criterion. Rings and the square referred to in the text.

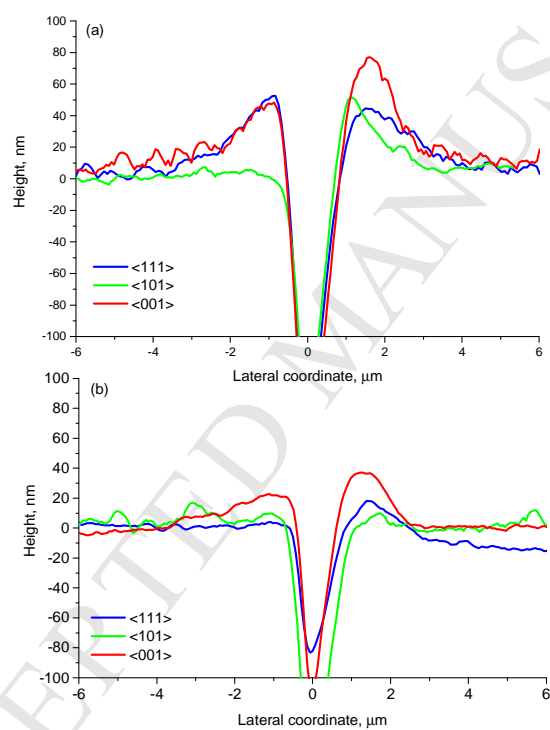


Fig. 4 Indent profilometry of reference sample: (a) deformed grains, (b) recrystallized grains.

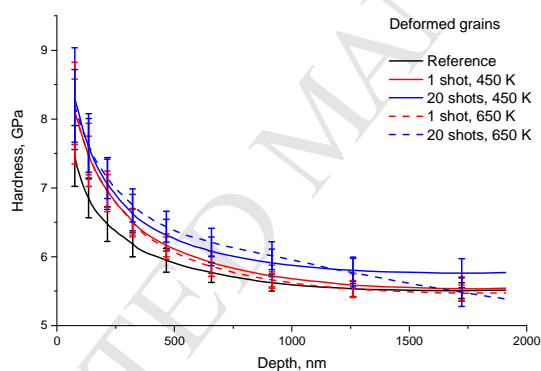


Fig. 5 Depth dependence of nanoindentation hardness measured on deformed grains, averaged for multiple indents, comparing unexposed samples, samples exposed to 1 reference shot and samples exposed to 20 reference shots.

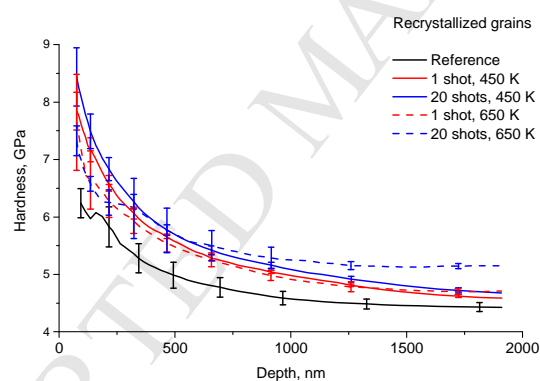


Fig. 6 Depth dependence of nanoindentation hardness measured on recrystallized grains, averaged for multiple indents, comparing unexposed samples, samples exposed to 1 reference shot and samples exposed to 20 reference shots.

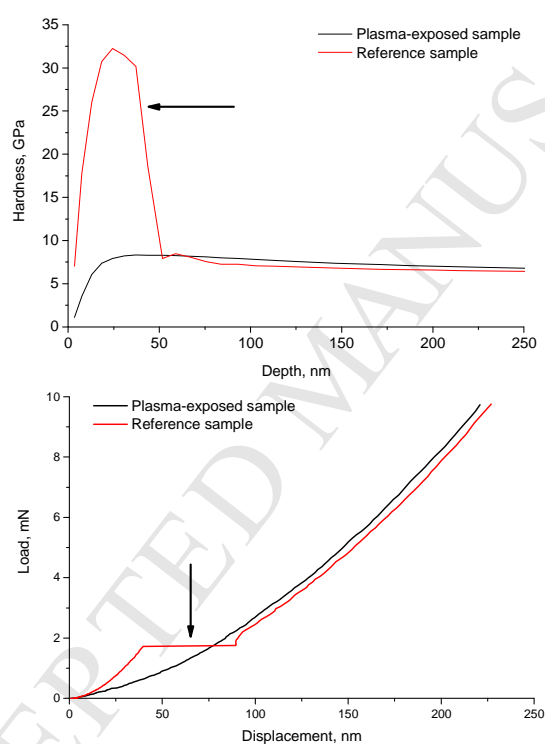


Fig. 7 Typical shape of near-surface hardness depth dependences and corresponding load-displacement curves, for reference and exposed samples.

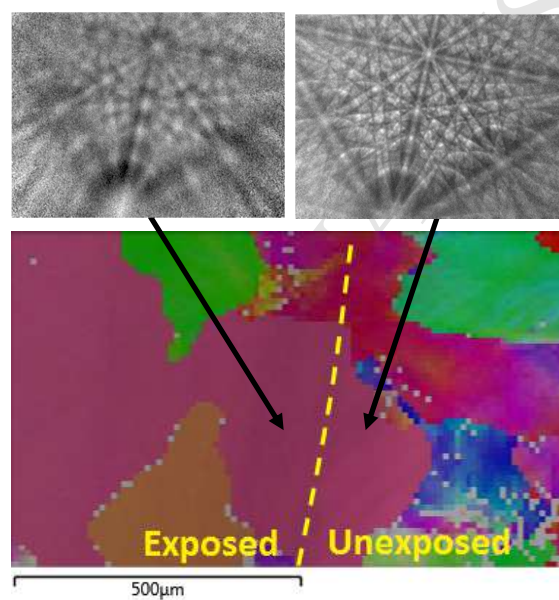


Fig. 8 Typical EBSD map of the vicinity of the boundary between exposed and unexposed (covered during the exposure) regions of a sample; boundary is denoted by the dashed line. Diffraction patterns correspond to the locations (denoted by arrows) within the same grain: its unexposed (right) and exposed (left) parts.

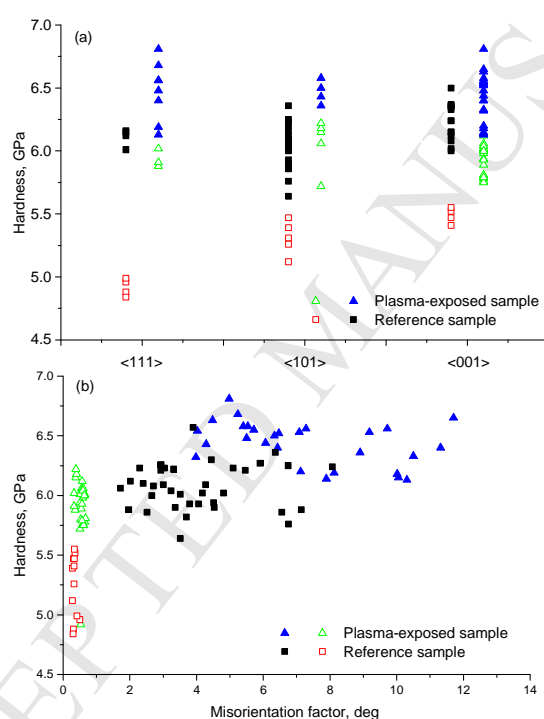


Fig. 9 Dependence of hardness for reference and plasma-exposed samples, averaged over the depth range of 300 – 400 nm, on (a) crystallographic orientation and (b) misorientation factor.

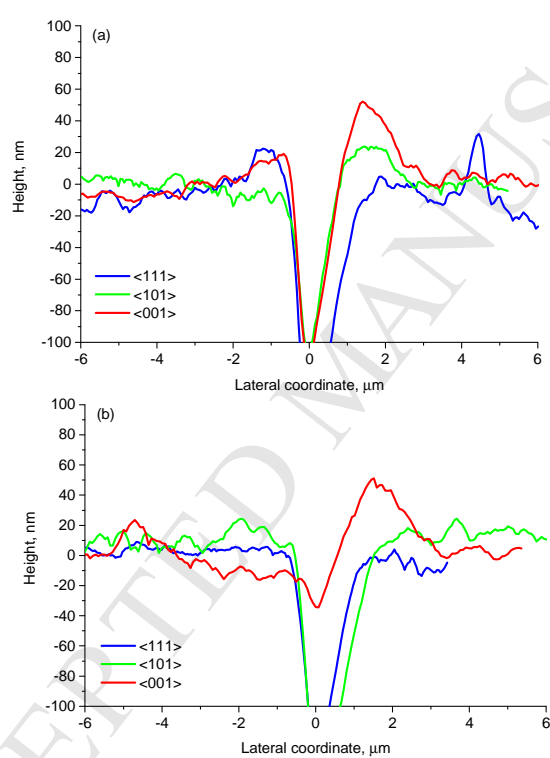


Fig. 10 Indent profilometry of plasma-exposed sample – (a) deformed grains, (b) recrystallized grains.